Abdominal Radiology

Published online: 6 October 2018

Abdom Radiol (2019) 44:867–876
https://doi.org/10.1007/s00261-018-1803-x

Differentiation of duodenal gastrointestinal stromal tumors from hypervascular pancreatic neuroendocrine tumors in the pancreatic head using contrast-enhanced computed tomography

Shuai Ren,[1] Xiao Chen,[1] Jianhua Wang,[1] Rui Zhao,[1] Lina Song,[1] Hui Li,[2] and Zhongqiu Wang[1]

[1]Department of Radiology, The Affiliated Hospital of Nanjing University of Chinese Medicine, No. 155 Hanzhong Road, Nanjing 210029, Jiangsu Province, China
[2]Department of Pathology, The Affiliated Hospital of Nanjing University of Chinese Medicine, Nanjing 210029, Jiangsu Province, China

Abstract

Purpose: To determine useful contrast-enhanced computed tomography (CE-CT) features in differentiating duodenal gastrointestinal stromal tumors (duodenal GISTs) from hypervascular pancreatic neuroendocrine tumors in the pancreatic head (pancreatic head NETs).
Methods: Seventeen patients with pathologically confirmed duodenal GISTs and 25 with pancreatic NETs underwent preoperative CE-CT. CT image analysis included tumor size, morphology, and contrast enhancement. Receiver operating characteristic curves were performed, and cutoff values were calculated to determine CT findings with high sensitivity and specificity.
Results: CT imaging showed duodenal GISTs with higher frequencies of tumor central location close to the duodenum and a predominantly solid tumor type when compared with pancreatic head NETs ($p < 0.05$ for both). Duodenal GISTs were larger than pancreatic head NETs (3.3 ± 0.9 cm vs. 2.5 ± 1.1 cm, $p = 0.03$). Duodenal GISTs had significantly lower CT attenuation values (112.9 ± 17.9HU vs. 137.4 ± 32.1HU, $p < 0.01$) at the arterial phase and higher CT attenuation values at the delayed phase (94.3 ± 7.9HU vs. 84.9 ± 10.4HU, $p < 0.01$) when compared with pancreatic head NETs. A CT attenuation value of ≤ 135 HU at the arterial phase (30 s) was 76% sensitive, 94.1% specific, and 83.3% accurate for the diagnosis of duodenal GISTs, while a CT attenuation value of ≥ 89.5 HU at the delayed phase (120 s) was 93.3% sensitive, 81.8% specific, and 76.2% accurate for the diagnosis of duodenal GISTs.
Conclusion: Tumor central location, size, texture, and contrast enhancement are valuable characteristics for the differentiation between duodenal GISTs and hypervascular pancreatic head NETs during preoperative examination.

Key words: Gastrointestinal stromal tumors—Duodenum—Neuroendocrine tumors—Pancreas—Computed tomography

Gastrointestinal stromal tumors (GISTs) account for approximately one-fifth of soft-tissue sarcomas with an annual incidence of approximately 10 per million population [1, 2]. GISTs may arise in any part of the gastrointestinal tract, but mostly occur in the stomach (50–60%), small intestine (20–30%), and colorectal region (10%) [3]. Only 3–5% of GISTs occur in the duodenum [4]. If GISTs arise from the C loop of the duodenum, they are difficult to differentiate from a pancreatic head mass because of anatomical proximity [5, 6]. GISTs are

Shuai Ren and Xiao Chen have contributed equally to this work.

Electronic supplementary material The online version of this article (https://doi.org/10.1007/s00261-018-1803-x) contains supplementary material, which is available to authorized users.

Correspondence to: Zhongqiu Wang; *email:* zhqwang001@126.com

often hypervascular tumors and demonstrate a hypervascular pattern in the multiphasic dynamic computed tomography (CT) or magnetic resonance imaging (MRI) [7]. Pancreatic neuroendocrine tumors (pancreatic NETs) also demonstrate a hypervascular pattern on CT or MRI imaging [8, 9]. Therefore, close proximity of duodenal GISTs to pancreatic head often mimics hypervascular pancreatic head NETs [4, 5, 10, 11]. However, the treatment options and prognosis of GISTs and pancreatic NETs are substantially different, since GISTs exhibit a broad spectrum of clinical behaviors and the prognosis varies depending on the biological behaviors of GISTs [12]. Considering the high potential of malignancy associated with GISTs, complete surgical resection with negative microscopic margins should be considered as the standard treatment choice for resectable localized GISTs [13]. Moreover, adjuvant therapy with imatinib has been proposed for GIST surgical resection patients because of the substantial risk of relapse [6]. Pancreatic NETs are considered to be potentially malignant, but have a wide spectrum of aggressiveness and growth pattern [14]. Duodenum-preserving pancreatic head resections are increasingly performed for tumors located in the pancreatic head compared with classical pancreatic resections due to improvements in procedure-related morbidity [15]. In addition, somatostatin analogues, everolimus, and sunitinib can prolong progression-free survival in unresectable progressive cases of pancreatic NETs [16]. Due to differences in treatment options and surgical outcomes for these two tumors with close anatomical proximity, there is great clinical value in clearly differentiating duodenal GISTs from pancreatic head NETs with preoperative imaging.

Contrast-enhanced CT (CE-CT) is the primary imaging modality for evaluating patients with suspected pancreatic diseases [17–20]. A comprehensive analysis of the CT findings of duodenal GISTs compared with pancreatic head NETs would be of great value. To the best of our knowledge, no study has shown the role of CE-CT in distinguishing duodenal GISTs from pancreatic head NETs. Therefore, the purpose of this study was to investigate the potential for diagnostic differentiation between duodenal GISTs and pancreatic head NETs by CT imaging.

Materials and methods

Patients

The institutional review board approved this study, and patient informed consent was waived due to its retrospective nature. Forty-one patients with pathologically confirmed duodenal GISTs through needle biopsy or postoperative specimen between December 2013 and February 2017 were identified from two institutions. Exclusion criteria were as follows: (a) absence of preoperative CT examination or lack of dynamic CE-CT images (n = 9); or (b) tumor location far from the C loop of the duodenum (n = 15). A total of 17 patients (10 men and 7 women) with duodenal GISTs close to the C loop of the duodenum were included in our study (Fig. 1). The mean age was 54.2 ± 9.3 years (age range 39–77).

We also identified 76 patients with pathologically confirmed pancreatic NETs through needle biopsy or postoperative specimen between July 2012 and December 2016. Tumor masses that showed equal or greater enhancement level compared to the adjacent pancreatic parenchyma at the arterial phase were considered as hypervascular pancreatic NETs. Exclusion criteria were as follows: (a) absence of preoperative CT examination or lack of dynamic CE-CT images (n = 12); or (b) tumor located in the body or the tail of the pancreas (n = 18); (c) tumors not defined on preoperative CT (n = 5); or (d) tumors that showed a hypovascular pattern at the arterial phase (n = 16). A total of 25 patients (8 men and 17 women) with hypervascular pancreatic head NETs were included in our study (Fig. 1). The mean age was 50.7 ± 14.0 years (age range 28–79).

Pathological analysis

The tumor specimens were fixed in 10% formalin for 24 h. Then, the specimens were embedded in paraffin and sectioned for hematoxylin–eosin (H&E) staining (4 μm thick each sections). Immunohistochemistry was used to confirm the presence of pancreatic NETs by a pathologist with 14 years of experience in gastroenterology pathology. A comprehensive immunohistochemical analysis of chromogranin A (CgA), neuron-specific enolase (NSE), and synaptophysin (Syn) was conducted,

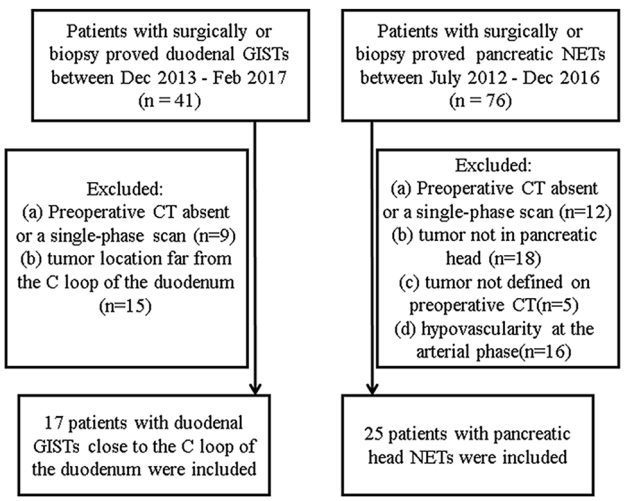

Fig. 1. Flow diagram of study group inclusion process. Duodenal GISTs, duodenal gastrointestinal stromal tumors; Pancreatic NETs, pancreatic neuroendocrine tumors; CT, computed tomography.

and pathological tumor grades of pancreatic NETs were determined by counting the number of mitoses per 10 high-power fields and detecting the Ki-67 proliferation index according to the WHO 2010 classification [21]. Tumors from 23 patients were classified as G1 NETs and two were G2 NETs. GISTs were confirmed with immunohistochemistry and histopathological examination of specimens obtained after surgery or from biopsy by detecting the presence of GIST-associated markers CD117, CD34, and DOG-1 in tissue samples.

CT imaging technique

Pathologically diagnosed patients underwent multidetector spiral CT examination (Philips Brilliance 64; Philips Healthcare, DA Best, the Netherlands, $n = 29$; or Lightspeed, VCT, or Discovery HD750, GE Healthcare, Milwaukee, WI, USA, $n = 13$). After a plain CT scan, all patients received a contrast media dosage (Omnipaque 350 mg I/mL at 1.2 mL/kg body weight, GE Healthcare) at a rate of 3.0 mL/s followed by 40 mL saline solution into an elbow vein via a power injector. All CT scanning parameters were as follows: tube voltage of 120 kVp, tube current of 240–300 mAs, helical pitch of 1.375, gantry rotation time of 0.5 s, slice thickness of 3.0 mm, slice interval of 3.0 mm, and a reconstruction interval of 1.25 mm. Fifteen patients with duodenal GISTs and 22 with pancreatic head NETs underwent a 4-phase CT examination (unenhanced, arterial, portal venous, and delayed phase). The other 2 patients with duodenal GISTs and 3 with pancreatic head NETs underwent a 3-phase CT examination (unenhanced, arterial, and portal venous phase). The enhanced images were collected at 30 s for the arterial phase, 60 s for the portal venous phase, and 120 s for the delayed phase imaging.

Qualitative and quantitative CT image analysis

Two radiologists (with 6 and 8 years of experience in abdominal radiology) with no prior knowledge of detailed histopathological information of any patients reviewed CT images independently. Consensus was reached through discussion or by referral to a third radiologist (with 13 years of experience in abdominal radiology). Features evaluated on the CT images included tumor central location (close to the duodenum, close to the pancreatic head, or uncertain), tumor margin, texture, calcification, and pancreatic duct dilatation. Tumor central location was evaluated based on the axial images with the largest cross-sectional area of the tumor and the reconstructed coronal images. A well-defined margin was defined as a smooth and clearly visible margin. A poorly defined margin was defined as spiculation or infiltration on $> 90°$ of the tumor perimeter [22]. Tumor texture was divided into solid (cystic or necrotic component of less than 10%), predominantly solid (cystic or necrotic component of 10–50%), and predominantly cystic (cystic or necrotic component of more than 50%) [23]. The cystic or necrotic components in the tumor were defined as either possessing CT attenuation < 20 Hounsfield units (HU) on unenhanced images or by the absence of enhancement on contrast-enhanced images. Pancreatic duct dilatation was defined as a diameter ≥ 4 mm [24].

The tumor size [centimeter (cm)] and CT attenuation values (HU) of the tumors were measured at each phase by another radiologist (with 15 years of experience in abdominal radiology). CT attenuation values of the tumors were determined by drawing a region of interest (ROI) in the solid part of tumor showing the most remarkable enhancement as large as possible (at least 30 mm^2) avoiding intratumoral calcification and cystic or necrotic components. The ROI was placed on the same equivalent site for each phase CT. Each ROI measured 3 times, and the average value was calculated.

Statistical analysis

A kappa analysis was used to evaluate interobserver agreement. Categorical variables were presented as the number of cases (percentage) and were analyzed by using Chi-square or Fisher's exact tests. Quantitative variables were presented as mean ± SD and were analyzed using a Mann–Whitney U test. The receiver operating characteristic (ROC) curve was generated to assess diagnostic performance and determine the optimal cutoff values for the most significant CT findings that could be used to differentiate duodenal GISTs from pancreatic head NETs. The sensitivity, specificity, positive predictive value (PPV), negative predictive value (NPV), and accuracy for the differentiation between duodenal GISTs and pancreatic head NETs were measured for each parameter. A p value < 0.05 was considered a significant statistical difference. All statistical analyses were performed using SPSS (version 19.0 IBM Corp. IBM SPSS Statistics for Windows).

Results

Clinical data

All clinical data are shown in Table 1. Seventeen patients with pathologically confirmed duodenal GISTs through needle biopsy (4 cases) or surgery (13 cases) and 25 patients with pathologically confirmed pancreatic head NETs through needle biopsy (10 cases) or surgery (15 cases) were included and compared in our study. No difference was found for demographic data or clinical symptoms between the two groups. However, diarrhea or abdominal bloating was more common in patients with pancreatic head NETs compared with duodenal GIST patients (56% vs. 23.5%, $p > 0.05$). Functioning tumors

Table 1. Clinical characteristics of patients with duodenal gastrointestinal stromal tumors (duodenal GISTs) and those with hypervascular pancreatic neuroendocrine tumors in pancreatic head (pancreatic head NETs)

Characteristics	Duodenal GISTs (n = 17)	Pancreatic head NETs (n = 25)	p values
Age (years)[a]	54.2 ± 9.3	50.7 ± 14.0	0.36[b]
Gender			
Male	10/17 (58.8%)	8/25 (32.0%)	0.09
Female	7/17 (41.2%)	17/25 (68.0%)	
Clinical symptoms			
Abdominal pain	10/17 (58.8%)	15/25 (60.0%)	0.94
Diarrhea or abdominal bloating	4/17 (23.5%)	14/25 (56.0%)	0.08
Yellow urine or icterus	1/17 (5.90%)	3/25 (12.0%)	0.90
Marasmus	1/17 (5.90%)	0 (0.0%)	0.84
Others	4/17 (23.5%)	3/25 (12.0%)	0.57
Asymptomatic	5/17 (29.4%)	6/25 (24.0%)	0.70
Pathology			0.44
Surgery	13 (76.5%)	15 (60.0%)	
Biopsy	4 (23.5%)	10 (40%)	

Unless otherwise specified, data are the number of patients and data in parentheses are the percentages
[a]Data are presented as average ± standard deviations
[b]Represents quantitative variables

were found in 4 patients with pancreatic NETs: 2 insulinomas, 1 glucagonoma, and 1 somatostatinoma.

CT findings: qualitative and quantitative analysis

The interobserver agreements ranged from moderate to near perfect (κ = 0.75 for tumor central location, κ = 0.81 for tumor margin, κ = 0.90 for tumor texture, κ = 1.0 for calcification, and κ = 0.79 for upstream pancreatic duct dilatation).

CT findings of duodenal GISTs and pancreatic head NETs are summarized in Table 2. No significant difference was observed with respect to tumor margin, calcification, or pancreatic duct dilatation. There was a significant difference in tumor central location between the two groups ($p < 0.01$). Closer proximity to the duodenum was more common in duodenal GISTs compared with pancreatic head NETs (58.8% vs. 8.0%). Figure 2 shows that tumor central location is close to the third portion of the duodenum, a typical case in duodenal GISTs. Figure 3 shows a typical case in pancreatic head NETs, of which tumor central location is close to the pancreatic head. In addition, our study demonstrated that duodenal GISTs showed a higher frequency of a predominantly solid tumor type compared with pancreatic head NETs (58.8% vs. 24.0%, p = 0.02). Supplemental Figs. 1 and 2 demonstrate two cases of pancreatic head NETs and duodenal GISTs, respectively.

The size (mean ± SD) and CT attenuation values (mean ± SD) of duodenal GISTs and pancreatic head NETs are shown in Table 2. The mean size of duodenal GISTs was larger than that of pancreatic head NETs (3.3 ± 0.9 cm vs. 2.5 ± 1.1 cm, p = 0.03). The enhancement level of duodenal GISTs was significantly lower than that of pancreatic head NETs at the arterial phase (112.9 ± 17.9 HU vs. 137.4 ± 32.1 HU, $p < 0.01$). The enhancement level of duodenal GISTs at the delayed phases was significantly higher than that of pancreatic head NETs (94.3 ± 7.9 HU vs. 84.9 ± 10.4 HU, $p < 0.01$). The comparisons of tumor size and contrast enhancement at the arterial phase between duodenal GISTs and pancreatic head NETs are demonstrated in Fig. 4. Figure 5 shows that enhancements of duodenal GISTs and pancreatic head NETs reached peak values at the arterial phase, and CT attenuation values of the two groups showed a washout pattern at the portal venous phase.

Imaging feature diagnostic performance

We subsequently assessed the diagnostic performance of the CT findings in differentiating duodenal GISTs from pancreatic head NETs (Table 3). The area under the curve (AUC) ranged from 0.674 to 0.862. The sensitivity and specificity ranged from 58.9% to 93.3% and from 58.8% to 94.1%, respectively. The accuracies with tumor central location, tumor texture, mean tumor size, CT attenuation values at the arterial phase (ACE), and delayed phase (DCE) ranged from 64.3% to 86.3%. The positive and negative predicative values ranged from 55.6% to 95.0% and 62.5% to 94.7%, respectively.

The sensitivity and specificity of each cutoff value and ROC analysis of the tumor size, ACE, and DCE are summarized in Fig. 6. The optimal cutoff value of 2.75 cm of tumor size was determined by maximizing the sum of sensitivity and specificity with 82.4 sensitivity, 72 specificity, and 76.2 accuracy. The optimal cutoff value of 135 HU was determined at the arterial phase with 76 sensitivity, 94.1 specificity, and 83.3 accuracy, and 89.5 HU at the delayed phase with 93.3 sensitivity, 81.8

Table 2. Comparisons of CT findings between duodenal gastrointestinal stromal tumors (duodenal GISTs) and those with hypervascular pancreatic neuroendocrine tumors in pancreatic head (pancreatic head NETs)

CT findings	Duodenal GISTs (n = 17)	Pancreatic head NETs (n = 25)	p values
Mean tumor size (cm)[a]	3.3 ± 0.9 (1.9–5.2)	2.5 ± 1.1 (1.1–5.8)	0.03[b]
Tumor central location			< 0.01
Close to the pancreatic head	2/17 (11.8%)	17/25 (68.0%)	
Close to the duodenum	10/17 (58.8%)	2/25 (8.0%)	
Uncertain	5/17 (29.4%)	6/25(24.0%)	
Tumor margin			0.95
Well-defined	14/17 (82.4%)	22/25 (88.0%)	
Ill-defined	3/17 (17.6%)	3/25 (12.0%)	
Tumor texture			0.02
Solid	7/17 (41.2%)	19/25 (76.0%)	
Predominantly solid	10/17 (58.8%)	6/25 (24.0%)	
Predominantly cystic	0/17 (0.0%)	0/25 (0.0%)	
Calcification			0.41
Present	1/17 (5.9%)	0/25 (0.0%)	
Absent	16/17 (94.1%)	25/25 (100.0%)	
Pancreatic duct dilatation			0.51
Present	0/17 (0.0%)	2/25 (8.0%)	
Absent	17/17 (100.0%)	23/25 (92.0%)	
CT contrast enhancement (HU)[a]			
Arterial phase	112.9 ± 17.9	137.4 ± 32.1	< 0.01
Portal venous phase	100.9 ± 13.3	109.4 ± 23.0	0.12
Delayed phase	94.3 ± 7.9	84.9 ± 10.4	< 0.01

Unless otherwise specified, data are the number of patients and data in parentheses are the percentages
HU, Hounsfield unit
[a]Data are presented as average ± standard deviations
[b]Represents quantitative variables

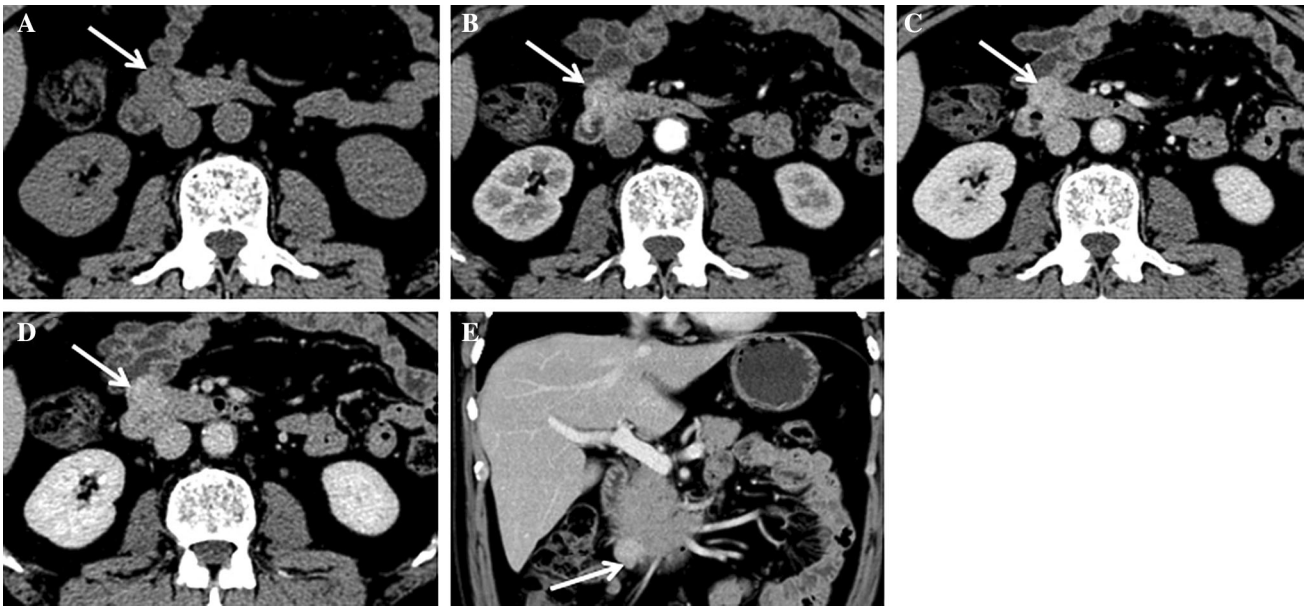

Fig. 2. CT images in a 69-year-old woman with duodenal GISTs. **A** Unenhanced axial CT image demonstrates an isoattenuating mass (arrows) between the third portion of duodenum and the processus uncinatus of the pancreas. **B**–**D** Arterial phase (**B**), portal venous phase (**C**), and delayed phase (**D**) CT images reveal a 1.4-cm well-defined, hyperattenuating tumor compared with the adjacent parenchyma (arrows). **E** Coronal CT image shows a hyperintense enhancing mass (arrows), and tumor central location is close to the third portion of the duodenum.

specificity, and 76.2 accuracy for the differential diagnosis of duodenal GISTs from pancreatic head NETs. Tumor size, ACE, and DCE showed the acceptable accuracies, sensitivities, and specificities.

Discussion

Duodenal GISTs and pancreatic head NETs are hypervascular tumors and often demonstrate avid enhancement at the arterial phase and can become cystic or

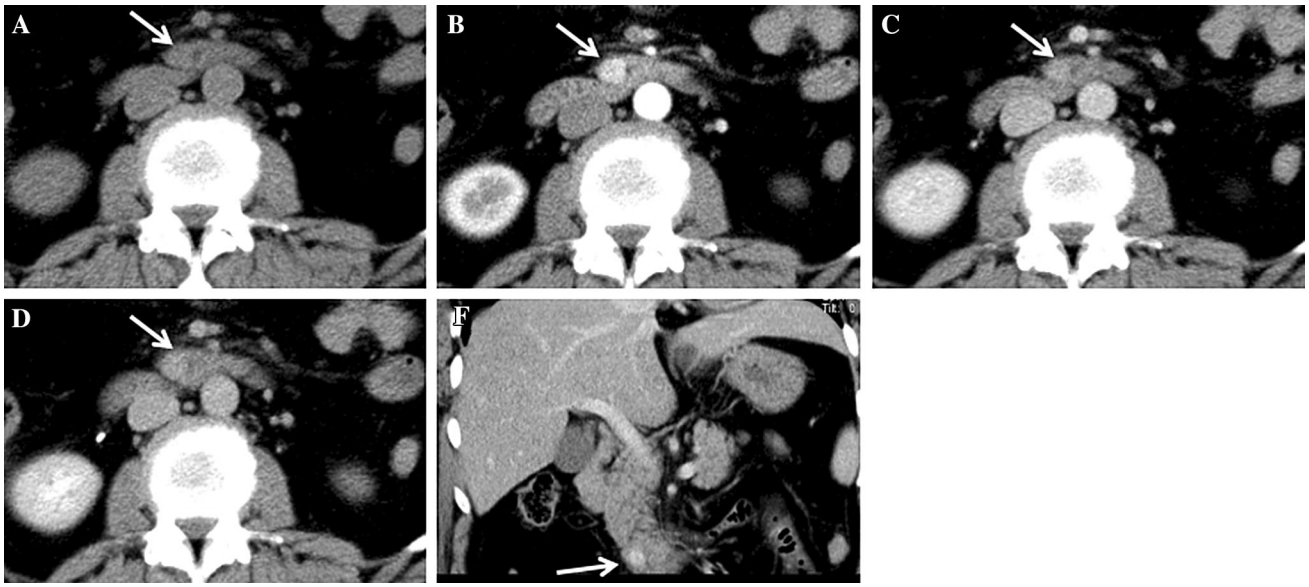

Fig. 3. CT images in a 56-year-old woman with pancreatic head NET. **A** Unenhanced axial CT image shows an isodense mass (arrows) between the third portion of duodenum and the processus uncinatus of the pancreas. **B**, **C** Arterial phase (**B**) and portal venous phase (**C**) CT images show a 2.0-cm well-defined, hyperattenuating tumor compared with the adjacent parenchyma (arrows). **D** The tumor shows isoattenuation in the delayed phase. **E** Coronal image shows a hyperintense enhancing mass (arrows), and tumor central location is close to the processus uncinatus of the pancreas.

necrotic in appearance as they grow larger [25–27]. Moreover, when duodenal GISTs grow outward exophytically from the duodenum toward the pancreatic head, they are very difficult to differentiate from pancreatic head NETs [25]. However, treatment approaches for patients with duodenal GISTs and pancreatic head NETs are different. Pancreas-sparing duodenectomy may be indicated for duodenal GISTs involving the second portion of the duodenum [13], while duodenum-preserving pancreatic head resections may be proposed for pancreatic head NETs [15]. It is vital to preoperatively distinguish GIST and pancreatic head NET tumors. Our results demonstrate that two qualitative CT findings, including tumor central location and texture, and three quantitative CT findings, including tumor size, ACE, and DCE, are statistically significant predictors in the differentiation of those two tumors.

Cai et al. [28] reported that 94.1% of duodenal GISTs showed a well-defined margin and that calcification was less common in duodenal GISTs (8.8%). Park et al. [29] reported that 100% of pancreatic head NETs showed a well-defined margin, in which calcification was detected with a frequency of 13.3%. Moreover, only 23.3% of pancreatic head NETs presented with pancreatic duct dilatation. In our study, 82.4% of duodenal GISTs and 88% of pancreatic head NETs had a well-defined margin, which was consistent with previous studies [28, 29]. Notably, both duodenal GISTs and pancreatic head NETs showed lower frequencies of calcification and pancreatic duct dilatation. There were no significant differences in tumor margin, calcification, or pancreatic duct dilatation between the two tumors.

However, there were significant differences with respect to tumor central location, size, and texture between duodenal GISTs and pancreatic head NETs. Duodenal GISTs most frequently involve the second portion of the duodenum, followed by the third portion, fourth portion, and first portion [11]. It is challenging to differentiate duodenal GISTs involving the second or the third portion of the duodenum from a pancreatic head mass because of the adjacent anatomical sites. Accurate diagnosis is typically contingent upon identifying the remaining fat plane between the tumor itself and the adjacent pancreas or the adjacent gastrointestinal wall [30, 31]. Combined with axial CT images, multiplanar reformation (MPR), especially coronal images, may provide us with more detail about the origin of the mass, as we can more clearly observe the spatial relationship between the tumor and duodenum or pancreatic head. In our study, we found that duodenal GISTs showed a higher frequency of being close to the duodenum when compared with pancreatic head NETs. However, determining the precise origin of the tumor when it was located between the duodenum and pancreatic head, or when it was too large to be delineated on images, was difficult. Moreover, we observed that the mean size of duodenal GISTs was larger than that of pancreatic head NETs. Cai et al. [28] reported that 61.8% of duodenal

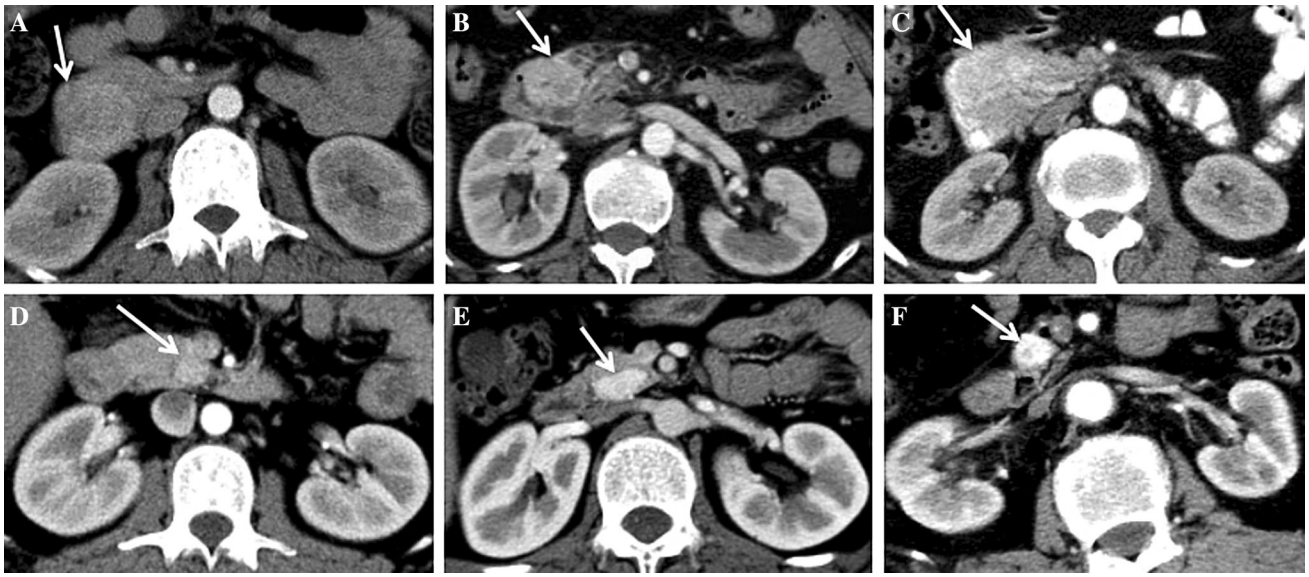

Fig. 4. Comparisons of contrast enhancement levels at the arterial phase between duodenal GISTs (**A**–**C**) and pancreatic head NETs (**D**–**F**) for six patients. The CT attenuation values of all 3 duodenal GISTs were lower than those of 3 cases of pancreatic head NETs at the arterial phase. The mean size of all 3 duodenal GISTs was larger than that of 3 cases of pancreatic head NETs. **A** 69-year-old woman with a 3.5-cm round hyperdense mass (arrows) between the third portion of duodenum and the processus uncinatus of the pancreas, and tumor central location is close to the third portion of the duodenum. CT attenuation value of the tumor is 108HU. **B** 39-year-old woman with a 2.9-cm oval hyperdense mass (arrows) between the inner wall of the duodenum and the pancreatic head, and tumor central location is uncertain. CT attenuation value of the tumor is 110HU. **C** 63-year-old man with a 6.2-cm round hyperdense mass (arrows), the origin of tumor cannot be defined as the tumor is too large. CT attenuation value is 115HU. **D** 30-year-old woman with a 1.5-cm round hyperattenuating mass (arrows) between the third portion of the duodenum and the processus uncinatus of the pancreas, and tumor central location is uncertain. CT attenuation value of the tumor is 126HU. **E** 28-year-old woman with a 2.2-cm oval hyperattenuating mass (arrows) between the third portion of the duodenum and the processus uncinatus of the pancreas, and tumor central location is close to the pancreatic head, and CT attenuation value of the tumor is 206HU. **F** 79-year-old woman with a 1.8-cm round hyperattenuating mass (arrows) close to the duodenum. CT attenuation value of the tumor is 160HU.

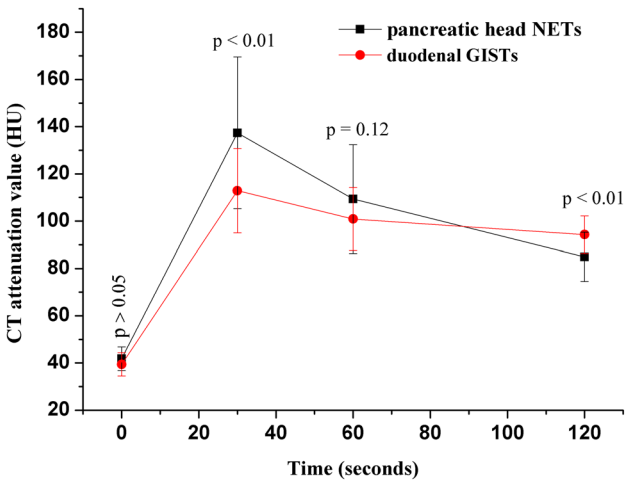

Fig. 5. Patterns of enhancement on multiphasic imaging of duodenal GISTs and pancreatic head NETs. The CT attenuation values of duodenal GISTs and pancreatic head NETs were 39.4 ± 4.9 HU and 41.8 ± 5.0 HU on unenhanced CT images, respectively. The curves represent attenuation values (mean ± SD) for each phase.

GISTs presented with necrosis or cystic degeneration. In our cases, 58.8% of duodenal GISTs were defined as predominantly solid tumors, which was consistent with previous reports. Takumi et al. [32] reported that cystic or necrotic degeneration could be seen in 18.5% of pancreatic NETs. Our study showed that 24% of pancreatic head NETs were defined as predominantly solid tumors, and the frequency was significantly lower than that of duodenal GISTs.

Previous studies compared the enhancement patterns of GISTs and NETs originating from the small bowel [7]; however, no study compared the enhancement patterns of duodenal GISTs and pancreatic head NETs. It was reported that duodenal GISTs usually show rapid enhancement followed by washout at the portal venous phase [7] and that hypervascular pancreatic NETs usually reach peak attenuation at the arterial phase followed by washout at the portal venous phase [32]. In our study, the enhancement patterns demonstrated that both duodenal GISTs and pancreatic head NETs reached the peak attenuation at the arterial phase, followed by a washout at the portal venous phase. A similar trend was observed in these two tumors. However, based on the calculation

Table 3. Diagnostic performances of CT imaging features

Variables	AUC	Sensitivity (95% CI) (%)	Specificity (95% CI) (%)	PPV (%)	NPV (%)	Accuracy (%)
Tumor central location	0.722	58.9 (33.5–80.6)	68.0 (46.4–84.3)	55.6	70.8	64.3
Tumor texture	0.674	76.0 (54.5–89.8)	58.8 (33.5–80.6)	73.1	62.5	69.0
Mean tumor size	0.779	82.4 (55.8–95.3)	72.0 (50.4–87.1)	66.7	85.7	76.2
ACE	0.819	76.0 (54.5–89.8)	94.1 (69.2–99.7)	95	72.7	83.3
DCE	0.862	93.3 (66.0–99.7)	81.8 (59.0–94.0)	77.8	94.7	76.2

AUC, area under curve; PPV, positive predictive value; NPV, negative predictive value; ACE, arterial contrast enhancement; DCE, delayed contrast enhancement; CI, confidence interval

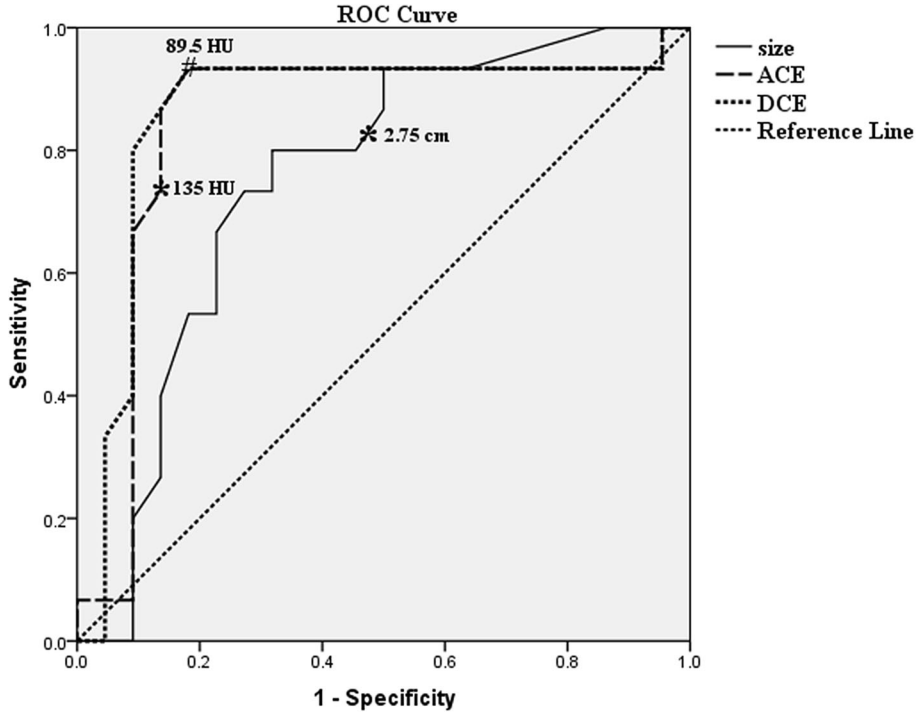

Fig. 6. Receiver operating characteristic (ROC) curves of the tumor size, CT contrast enhancement in the arterial phase (ACE), and delayed phase (DCE) for differentiating duodenal GISTs from pancreatic head NETs.

of enhancement levels, an arterial threshold of 135 HU and a delayed threshold of 89.5 HU can be used to differentiate duodenal GISTs from pancreatic head NETs. A CT attenuation value of ≤ 135 HU at the arterial phase was 76% sensitive, 94.1% specific, and 83.3% accurate for the diagnosis of duodenal GISTs vs. pancreatic head NETs, while a CT attenuation value of ≥ 89.5 HU at the delayed phase was 93.3% sensitive, 81.8% specific, and 76.2% accurate for the diagnosis of those two tumors. Generally speaking, a pancreatic parenchymal phase (40 or 45 s) and a portal venous phase (65 or 70 s) are more common for pancreas during CE-CT examination. However, considering that the late arterial (30 s) or pancreatic parenchymal phase (40 s) is mandatory allowing an increased detection of small functioning PNET in particular for insulinoma [33], a routine scan delays consisting of an arterial phase (30 s), a portal venous phase (60 s), and/or a delayed phase (120 s) are performed for pancreas examination in our institution. In addition, late arterial or pancreatic parenchymal phase can also increase the detection of hepatic metastases [34]. According to the time-density curves of 2 entities in our study, the enhancement levels of pancreatic head NETs were significantly higher than those of duodenal GISTs at the arterial (30 s) and portal phase (60 s); Hence, the estimated enhancement level of pancreatic head NETs may be significantly higher than that of duodenal GISTs at pancreatic parenchymal phase (40 or 45 s). Our study indicates that the enhancement levels on multiphasic CT can provide a simpler, less invasive method of performing the differential diagnosis of these two tumors.

Although our study is the first to evaluate CE-CT findings in differentiating duodenal GISTs from pancreatic head NETs, there are several possible limitations. First, our patients underwent CT examinations with various CT scanners. These limitations could not be avoided as the study itself was retrospective. Second,

our study included a relatively small number of patients. Despite the small number of patients, previous studies were solely case reports about a GIST of the duodenum misdiagnosed as a pancreatic head NET [4–6, 10, 11]. Third, we used a fixed-delay method for CE-CT, and the enhanced images were collected at 30 s for the arterial phase, not the so-called pancreatic parenchymal phase. Further studies comparing those two tumors at pancreatic parenchymal phase (40 or 45 s) are needed. Fourth, only CE-CT was investigated. The role of other imaging modalities, particularly endoscopic ultrasound-guided fine-needle aspiration (EUS-FNA) or hybrid techniques (e.g., octreotide SPECT) may be helpful in diagnosis of those two tumors [16, 35–37]. Although CE-CT, especially CT attenuation values, may provide us with clues to differentiate duodenal GISTs from pancreatic head NETs with a noninvasive method, it is also important to obtain tissue confirmation, e.g., biopsy. Our study is consequential for the possibility of distinguishing between the two tumors using CE-CT.

In conclusion, tumor central location close to the duodenum, a predominantly solid tumor type, size $>$ 2.75 cm, and a CT attenuation value of $\leq$ 135 HU at the arterial phase (30 s) and a CT attenuation value of $\geq$ 89.5 HU at the delayed phase (120 s) were shown to be useful CT findings with which to discriminate duodenal GISTs from hypervascular pancreatic head NETs.

Acknowledgments We thank all authors for their continuous and excellent support with patient data collection, imaging analysis, statistical analysis, and valuable suggestions for the article.

Compliance with ethical standards

Funding This study was supported by the Key Program of Research and Development of Jiangsu Province (BE2017772) and the National Natural Science Foundation of China (81471705; 81771899).

Conflict of interest The authors declare that they have no conflict of interest.

Informed content statement Patients were not required to give informed consent to the study because the analysis used anonymous clinical data that were obtained after each patient agreed to CE-CT examinations by written consent.

References

1. Joensuu H, Hohenberger P, Corless CL (2013) Gastrointestinal stromal tumour. Lancet 382:973–983
2. von Mehren M, Joensuu H (2018) Gastrointestinal stromal tumors. J Clin Oncol 36:136–143
3. Sugase T, Takahashi T, Nakajima K, et al. (2016) Clinicopathological characteristics, surgery and survival outcomes of patients with duodenal gastrointestinal stromal tumors. Digestion 94:30–36
4. Slavik T, Du Plessis J, Sparaco A, Van Der Merwe SW (2014) Duodenal gastrointestinal stromal tumor with epithelioid and neural features mimicking a primary pancreas head neuroendocrine tumor. Pancreas 43:482–483
5. Kwon SH, Cha HJ, Jung SW, et al. (2007) A gastrointestinal stromal tumor of the duodenum masquerading as a pancreatic head tumor. World J Gastroenterol 13:3396–3399
6. Vasile D, Iancu G, Iancu RC, Simion G, Ciuluvică RC (2017) Duodenal gastrointestinal stromal tumor presenting as pancreatic head mass: a case report. Rom J Morphol Embryol 58:255–259
7. Shinya T, Inai R, Tanaka T, et al. (2017) Small bowel neoplasms: enhancement patterns and differentiation using post-contrast multiphasic multidetector CT. Abdom Radiol 42:794–801
8. Zamboni GA, Ambrosetti MC, Zivelonghi C, et al. (2017) Solid non-functioning endocrine tumors of the pancreas: correlating computed tomography and pathology. HPB 19:986–991
9. Kim JH, Eun HW, Kim YJ, et al. (2016) Pancreatic neuroendocrine tumour (PNET): staging accuracy of MDCT and its diagnostic performance for the differentiation of PNET with uncommon CT findings from pancreatic adenocarcinoma. Eur Radiol 26:1338–1347
10. Bormann F, Wild W, Aksoy H, et al. (2014) A pancreatic head tumor arising as a duodenal GIST: a case report and review of the literature. Case Rep Med 2014:420295
11. Uchida H, Sasaki A, Iwaki K, et al. (2005) An extramural gastrointestinal stromal tumor of the duodenum mimicking a pancreatic head tumor. J Hepatobiliary Pancreat Surg 12:324–327
12. Kwon HJ (2010) Extra-gastrointestinal stromal tumor of the pancreas: report of a case. Ann Hepatobiliary Pancreat Surg 21:237–242
13. Valsangkar N, Sehdev A, Misra S, et al. (2015) Current management of gastrointestinal stromal tumors: surgery, current biomarkers, mutations, and therapy. Surgery 158:1149–1164
14. Sahani DV, Bonaffini PA, Fernández-Del Castillo C, Blake MA (2013) Gastroenteropancreatic neuroendocrine tumors: role of imaging in diagnosis and management. Radiology 266:38–61
15. Beger HG (2018) Benign tumors of the pancreas—radical surgery versus parenchyma-sparing local resection—the challenge facing surgeons. J Gastrointest Surg 22:562–566
16. Cloyd JM, Poultsides GA (2015) Non-functional neuroendocrine tumors of the pancreas: advances in diagnosis and management. World J Gastroenterol 21:9512–9525
17. Singhal S, Prabhu NK, Sethi P, Moorthy S (2017) Role of multi detector computed tomography (MDCT) in preoperative staging of pancreatic carcinoma. J Clin Diagn Res 11:TC01–TC05
18. Kim C, Byun JH, Hong SM, et al. (2017) A comparison of enhancement patterns on dynamic enhanced CT and survival between patients with pancreatic neuroendocrine tumors with and without intratumoral fibrosis. Abdom Radiol 42:2835–2842
19. Mönnings P, Belyaev O, Uhl W, et al. (2017) Criteria for determining malignancy in pancreatic intraductal papillary mucinous neoplasm based on computed tomography. Digestion 94:230–239
20. Jang SK, Kim JH, Joo I, et al. (2015) Differential diagnosis of pancreatic cancer from other solid tumours arising from the periampullary area on MDCT. Eur Radiol 25:2880–2888
21. Klimstra DS, Modlin IR, Coppola D, Lloyd RV, Suster S (2010) The pathologic classification of neuroendocrine tumors: a review of nomenclature, grading, and staging systems. Pancreas 39:707–712
22. Belousova E, Karmazanovsky G, Kriger A, et al. (2017) Contrast-enhanced MDCT in patients with pancreatic neuroendocrine tumours: correlation with histological findings and diagnostic performance in differentiation between tumour grades. Clin Radiol 72:150–158
23. Jeon SK, Lee JM, Joo I, et al. (2017) Nonhypervascular pancreatic neuroendocrine tumors: differential diagnosis from pancreatic ductal adenocarcinomas at MR imaging-retrospective cross-sectional study. Radiology 284:77–87
24. Kim DW, Kim HJ, Kim KW, et al. (2015) Neuroendocrine neoplasms of the pancreas at dynamic enhanced CT: comparison between grade 3 neuroendocrine carcinoma and grade 1/2 neuroendocrine tumour. Eur Radiol 25:1375–1383
25. Raman SP, Hruban RH, Cameron JL, Wolfgang CL, Fishman EK (2012) Pancreatic imaging mimics: part 2, pancreatic neuroendocrine tumors and their mimics. Am J Roentgenol 199:309–318
26. Verde F, Hruban RH, Fishman EK (2017) Small bowel gastrointestinal stromal tumors. J Comput Assist Tomogr 41:407–411
27. Miettinen M, Kopczynski J, Makhlouf HR, et al. (2003) Gastrointestinal stromal tumors, intramural leiomyomas, and leiomyosarcomas in the duodenum: a clinicopathologic, immunohistochemical, and molecular genetic study of 167 cases. Am J Surg Pathol 27:625–641
28. Cai PQ, Lv XF, Tian L, et al. (2015) CT characterization of duodenal gastrointestinal stromal tumors. Am J Roentgenol 204:988–993

29. Park HS, Kim SY, Hong SM, et al. (2016) Hypervascular solid-appearing serous cystic neoplasms of the pancreas: differential diagnosis with neuroendocrine tumours. Eur Radiol 26:1348–1358
30. Lee NK, Kim S, Kim GH, et al. (2010) Hypervascular subepithelial gastrointestinal masses: CT-pathologic correlation. RadioGraphics 30:1915–1934
31. Xue HD, Liu W, Xiao Y, et al. (2011) Pancreatic and peri-pancreatic lesions mimic pancreatic islet cell tumor in multidetector computed tomography. Chin Med J (Engl) 124:1720–1725
32. Takumi K, Fukukura Y, Higashi M, et al. (2015) Pancreatic neuroendocrine tumors: correlation between the contrast-enhanced computed tomography features and the pathological tumor grade. Eur J Radiol 84:1436–1443
33. Fidler JL, Fletcher JG, Reading CC, et al. (2003) Preoperative detection of pancreatic insulinomas on multiphasic helical CT. Am J Roentgenol 181:775–780
34. Dromain C, de Baere T, Lumbroso J, et al. (2005) Detection of liver metastases from endocrine tumors: a prospective comparison of somatostatin receptor scintigraphy, computed tomography, and magnetic resonance imaging. J Clin Oncol 23:70–78
35. Jilesen APJ, Hoefnagel SJM, Busch ORC, et al. (2016) The influence of somatostatin receptor scintigraphy during preoperative staging of non-functioning pancreatic neuroendocrine tumours. Clin Radiol 71:537–542
36. Koizumi S, Kida M, Yamauchi H, et al. (2016) Clinical implications of doubling time of gastrointestinal submucosal tumors. World J Gastroenterol 22:10015–10023
37. Boutsen L, Jouret-Mourin A, Borbath I, van Maanen A, Weynand B (2018) Accuracy of pancreatic neuroendocrine tumour grading by endoscopic ultrasound-guided fine needle aspiration: analysis of a large cohort and perspectives for improvement. Neuroendocrinology 106:158–166